Compositional modulation and optical emission in AlGaN epitaxial films

Min Gao[a] and S. T. Bradley
Department of Electrical and Computer Engineering, The Ohio State University, Columbus, Ohio 43210

Yu Cao and D. Jena
Department of Electrical Engineering, University of Notre Dame, Notre Dame, Indiana 46556

Y. Lin and S. A. Ringel
Department of Electrical and Computer Engineering, The Ohio State University, Columbus, Ohio 43210

J. Hwang and W. J. Schaff
Department of Electrical and Computer Engineering, Cornell University, Ithaca, New York 14853

L. J. Brillson
Department of Electrical and Computer Engineering, The Ohio State University, Columbus, Ohio 43210; Department of Physics, The Ohio State University, Columbus, Ohio 43210; and Center for Materials Research, The Ohio State University, Columbus, Ohio 43210

(Received 8 September 2006; accepted 15 September 2006; published online 20 November 2006)

Compositional, structural, and optical properties of molecular-beam epitaxy grown $Al_xGa_{1-x}N$ films were characterized by transmission electron microscopy (TEM), x-ray diffraction, and cathodoluminescence spectroscopy. Spontaneous modulation, phase separation, and band gap reductions were observed to vary systematically with AlN mole fraction across the full alloy series. At low AlN mole fraction ($x \leqslant 0.5$), AlGaN epilayers display pronounced phase separation. With increasing AlN mole fraction, phase separation is strongly suppressed by the formation of spontaneous modulation which high spatial resolution TEM techniques unambiguously determine to be atomic-scale compositional superlattice. The formation of the spontaneous superlattice is considered responsible for the pronounced reductions in band gaps and emission energies, exceeding several hundred meV for the Al-rich AlGaN, which has been confirmed by band structure calculations. © *2006 American Institute of Physics*. [DOI: 10.1063/1.2382622]

I. INTRODUCTION

AlGaN single crystal alloys are wide band gap semiconductors envisioned for numerous optoelectronic applications in the ultraviolet spectral region.[1–3] However, the key enabling aspect of such technologies, the growth of high-quality AlGaN films, has proven to be very challenging.[3,4] Due to the much lower mobility of Al versus Ga and the lack of a thermally and lattice-matched substrate, AlGaN films often suffer from extensive defects and cracking. The high donor and acceptor ionization energies result in low conductivity for both *n*- and *p*-doped in Al-rich AlGaN epilayers.[3] In addition, tailoring of the band gap with alloy composition has been difficult to predict theoretically. As summarized by Lee *et al.*, the band gap emission of AlGaN has been reported to vary over ~1 eV for the same alloy composition.[5] Especially pronounced are the reduced band gaps in the Al-rich regime.[5]

Compositional inhomogeneity, e.g., phase separation, spontaneous ordering, and compositional modulation, has been a critical issue for epitaxial semiconductor alloys and has attracted tremendous attention.[6–8] In contrast to InGaN, which exhibits a strong tendency toward spinodal phase separation,[2,9–18] AlGaN alloys are usually considered miscible above room temperature due to the small lattice mismatch between AlN and GaN.[2,13,16–18] On the other hand, spontaneous long range ordering structure has been reported in both AlGaN (Refs. 19–31) and InGaN (Refs. 9–13) grown by molecular-beam epitaxy (MBE) and metal organic chemical vapor deposition (MOCVD). The spontaneous long-range ordering (mostly 1:1 ordering, layer-by-layer alternation of the atoms in cation or anion sublattice along the [111] direction during growth along the [001] direction) has been shown to significantly modify the band gap and other electronic properties of cubic III–V alloys.[6–8] Both experiment[20,28,30] and calculation[31,32] showed that the 1:1 ordering in AlGaN, commonly considered to consist of alternating Ga–N and Al–N monolayers (ML), induced band gap reduction but that such reduction is less than 150 meV, i.e., much smaller than the reductions measured.[5] In contrast to the atomic ordering structure in traditional cubic III–V alloys, most reported ordering structures in AlGaN were along the [0001] axis (growth direction). In addition, besides the 1:1 ordering, epitaxial AlGaN films can exhibit more complex ordering with a variety of periods.[23,24,26,29,31] The satellite spots around the fundamental AlGaN reflections in electron diffraction patterns in transmission electron microscopy (TEM) and x-ray diffraction (XRD) have been the simplest indicator of the formation of the long range ordering and the main tools. Researchers concluded that such "complex ordering" was compositional ordering with Al-rich and Ga-rich layers or sometimes an AlN/GaN superlattice by ruling out other pos-

[a]Present address: Key Laboratory for the Physics and Chemistry of Nanodevices and Department of Electronics, Peking University, China; electronic mail: mingao@pku.edu.cn

TABLE I. AlGaN alloy compositions with their SIMS-measured impurity concentrations, CL-measured band gaps E_0, and emission peak energies E_x.

Sample No.	Al mole fraction x	Si concentration (at./cm^3)	O concentration (at./cm^3)	Si+O (at./cm^3)	E_0 (eV)	E_x (eV)
1	0.25	5.1×10^{18}	8.6×10^{18}	1.4×10^{19}	4.08	3.945
2	0.33	2.5×10^{19}	3.4×10^{19}	5.9×10^{19}	4.269	4.081
3	0.47	7.6×10^{19}	1.3×10^{19}	8.6×10^{19}	4.51	4.287
4	0.48	1.6×10^{19}	6.6×10^{18}	2.3×10^{19}	4.61	4.28
5	0.50	3.6×10^{18}	6.4×10^{18}	1×10^{19}	4.559	4.276
6	0.65	7.1×10^{19}	1.3×10^{19}	8.4×10^{19}	4.816	4.593
7	0.79	2.1×10^{19}	4.4×10^{20}	4.6×10^{20}	5.357	4.897
8	0.80	2.6×10^{19}	7.1×10^{20}	7.4×10^{20}	5.243	4.842
9	0.81	2.5×10^{19}	3.4×10^{20}	3.7×10^{20}	5.345	4.916
10	0.97	7.5×10^{19}	1.4×10^{20}	2.2×10^{20}	5.933	5.46
11	1	6.0×10^{19}	2.2×10^{19}	8.2×10^{19}	6.178	6.03

sibilities such as nitrogen vacancy ordering and stacking faults[23] and by comparing the simulated electron diffraction patterns to the experimental patterns.[21,26] As with the traditional III-V alloys,[6–8] the growth surface was found to play an important role in the formation of ordering and modulation structure in AlGaN. For example, in MBE-grown AlGaN, the 1:1 ordering is preferred under N-rich growth conditions, while group-III-rich conditions favor longer period modulation.[24]

In this study, we report measurements on MBE-grown $Al_xGa_{1-x}N$ samples with AlN mole fractions x extending across the full alloy series using high spatial resolution TEM, energy-dispersive x-ray spectroscopy (EDS), high resolution XRD, and cathodoluminescence spectroscopy (CLS) in an ultrahigh vacuum (UHV) scanning electron microscope (SEM). Our results provide direct evidence that the complex ordering is atomic compositional modulation. The systematic dependence of phase separation, spontaneous modulation, and near band edge (NBE) emission on alloy composition reveals a strong correlation between compositional modulation and the reductions of the NBE optical emission energies. First-principles calculations of the AlGaN band structure with atomic compositional modulations confirm the superlattice-induced band gap reductions and reveal the formation of minibands.

II. EXPERIMENT

A. Sample growth

AlGaN samples were grown in a turbomolecular pumped Varian Gen II MBE system using group III effusion cells and an EPI rf plasma source for nitrogen.[33] Substrates were 2 in. basal plane Al_2O_3 sapphire wafers covered with ~20 nm AlN buffer layers. A series of $Al_xGa_{1-x}N$ films (x =0.25–1.0) was grown at 800 °C under group-III-rich conditions. The substrate was heated with constant power instead of thermocouple feedback control to eliminate the possibility of substrate temperature oscillations. Table I shows AlN mole fractions, Si doping densities, and O densities of the 11 samples used in this study. All the AlGaN films (samples 1–11) were grown at the same rate of approximately 400 nm/h for 1 h. The wafers were rotated at 1 rpm throughout the growth for all the samples. AlN mole fractions were determined by high resolution double-axis and triple-axis XRD measurements using Vegard's law. Densities of Si and O were measured by secondary ion mass spectroscopy (SIMS).[34]

B. TEM specimen preparation and measurement

The cross-sectional TEM specimens were prepared by using a recently developed technique: combined *in situ* focused ion beam (FIB) and low-energy Ar ion milling. By using the 30 keV focused Ga ion beam, an Omniprobe micromanipulator, and the deposition of Pt as glue, a piece of sample ~2 μm in thickness and ~20 μm in length was cut free and glued to a finger of a specially designed half-open TEM grid from Omniprobe inside an FEI DB235 DualBeam system. Such a sample was then thinned down to ~200 nm in thickness followed by Ar ion milling at 2 keV and 4° using a Gatan PIPS ion miller. This technique combines the site-specific advantage of FIB and high surface quality of low-energy Ar ion milling. Our EDS and TEM imaging results (not shown) from pure AlN epilayer on sapphire substrate show that the low-energy Ar sputtering can remove any residual Ga and effectively reduce the surface damage introduced by the FIB. In addition, this technique has proven to be an easy preparation method for very brittle or very soft samples which are otherwise challenging for typical grinding/polishing/ion milling techniques, in particular, the brittle AlGaN/AlN/sapphire samples in this study.

We probed cross-sectional TEM specimens from samples 1 (x=0.25), 5 (0.50), 8 (0.80), 10 (=0.97), and 11 (1.0) using JEOL 2010F and FEI Tecnai TF20 microscopes. We employed a combination of reciprocal (electron diffraction) and real space techniques [high resolution TEM (HRTEM), Z-contrast imaging, and EDS line scan in scanning transmission electron microscopy (STEM) mode].

C. X-ray diffraction

A Bede D^1 diffractometer (four bounces) was used for high resolution double- and triple-axis XRD scans. A Philips X'pert diffractometer was ran under two-bounce mode to allow high intensity XRD scans, which improved signal/

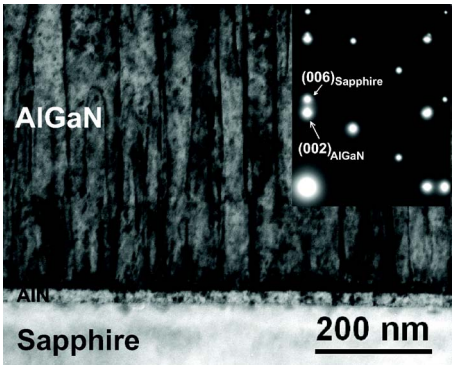

FIG. 1. (Color online) Cross-sectional TEM image of $Al_{0.25}Ga_{0.75}N/AlN/Al_2O_3$. The vertical dark lines inside the AlGaN film are inversion domain walls. The inset is a corresponding selected area electron diffraction pattern.

noise ratios and quantification of the modulation-related satellite peaks from samples with weak modulations.

D. Cathodoluminescence spectroscopy

We obtained micro-CLS in plan view for all samples at 12 K using an Oxford MonoCL monochromator and Hamamatsu photomultiplier attached to a JEOL 7800F UHV scanning Auger microscope.[34] The thin cross-sectional TEM specimens were also employed for CLS measurement, which dramatically reduced the beam spreading and allowed CLS measurement from nanometer-sized domains whose structure and composition can be measured by TEM and EDS.

III. RESULTS

A. Spontaneous composition modulation

Figure 1 shows a cross-sectional TEM image of $Al_{0.25}Ga_{0.75}N/AlN/Al_2O_3$. The main microstructure feature is the inversion boundaries. Dislocations were mainly found near the AlGaN/AlN interface. The corresponding electron diffraction pattern (Fig. 1 inset) shows no extra diffraction spots besides those from AlGaN, sapphire substrate, and the AlN buffer layer. Low magnification TEM images of AlGaN samples with higher Al concentration shows very similar microstructure features to those in Fig. 1, but spontaneous modulation can be observed by high resolution TEM (HRTEM), electron diffraction pattern, and XRD in Al-rich AlGaN epilayers. Figures 2(a) and 2(b) show cross-sectional HRTEM image and corresponding electron diffraction pattern of sample 8 (x=0.80), respectively. The existence of spontaneous modulation is evidenced by the dark lines separated periodically by 10 ML (~2.5 nm) in the HRTEM image and the satellite spots in the diffraction pattern.

We used low magnification and atomic resolution Z-contrast imaging (Fig. 3) and high spatial resolution EDS (Fig. 4) in a STEM to determine that the spontaneous modulation was that of an atomic compositional superlattice. A Z-contrast image can be considered to be a direct map of atomic locations with intensities strongly depending on the atomic number Z.[35] Figure 3(a) is a low magnification Z-contrast image showing that the composition modulation is very well defined. The modulation was found to spread

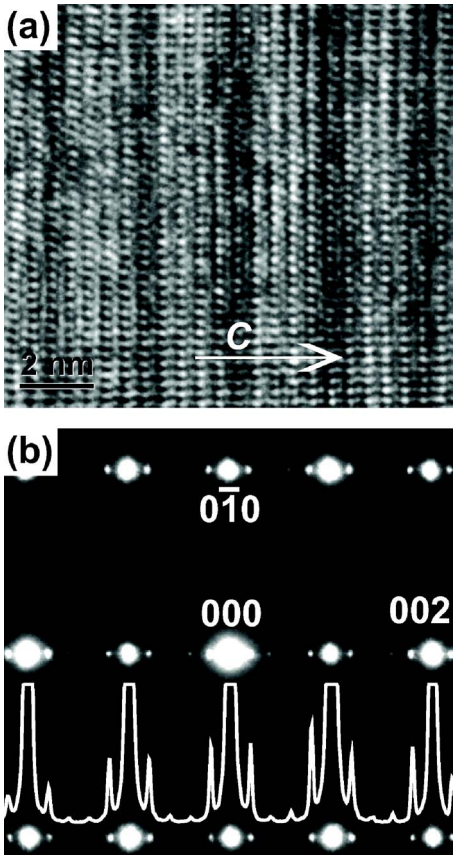

FIG. 2. (Color online) (a) Cross-sectional HRTEM image of $Al_{0.8}Ga_{0.2}N/AlN$/sapphire along [2$\bar{1}\bar{1}$0]. (b) Corresponding selected area electron diffraction pattern. Line scan in (b) shows corresponding intensity profile along the (0002) direction.

across the whole TEM specimens (>10 μm) with no evidence of fluctuation in the stacking sequence. The periodically varying contrast along the c axis in the atomic resolution Z-contrast image [Fig. 3(b)] shows directly that the spontaneous modulation is that of an atomic compositional superlattice consisting of alternating Ga-rich and Al-rich layers. It is shown in Fig. 3(b) that the domain boundary does not affect the modulation significantly and only causes a small shift (~ half ML) along the c axis. EDS spectra from Al-rich layer, Ga-rich layer, and large area (average) appear in Fig. 4(a). The Ga mole fraction variation [Fig. 4(b)] measured by high spatial resolution EDS line scans and the intensity profile [Fig. 3(b)] of the Z-contrast image in which each intensity peak corresponds to two atomic layers (one unit cell) indicate clearly that, instead of occupying two atomic layers in one modulation period (10 ML) to form an atomically abrupt GaN/AlN superlattice, Ga atoms spread across four to six atomic layers in a sinusoidal-like pattern, consistent with the very weak high order superlattice peaks in both electron diffraction [Fig. 2(a)] and XRD scans [Fig. 6(a)]. High spatial resolution EDS determined the AlN mole fraction maximum and minimum to be 0.952 and 0.679, respectively, i.e., a 27.3% variation in Al composition from maximum and minimum (modulation amplitude). The absolute error of our quantitative EDS measurement is ±2% (large area) or ±4% (subnanometer area) by using sample 1 with x=0.25 (determined to be 0.245 in average Al mole

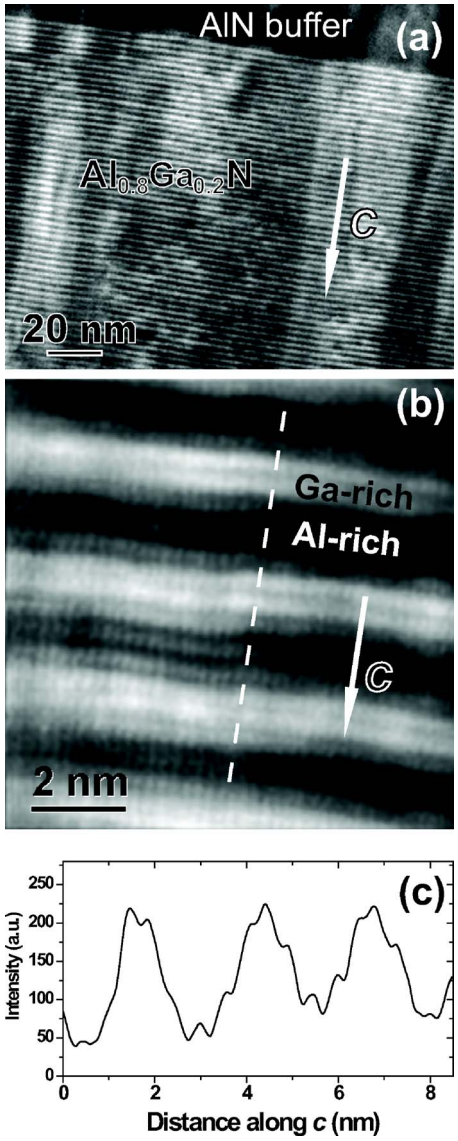

FIG. 3. (Color online) (a) Low and (b) high magnification Z-contrast images. In (b), a domain boundary is marked by a dashed line. (c) Intensity profile in the atomic resolution Z-contrast image along the growth direction.

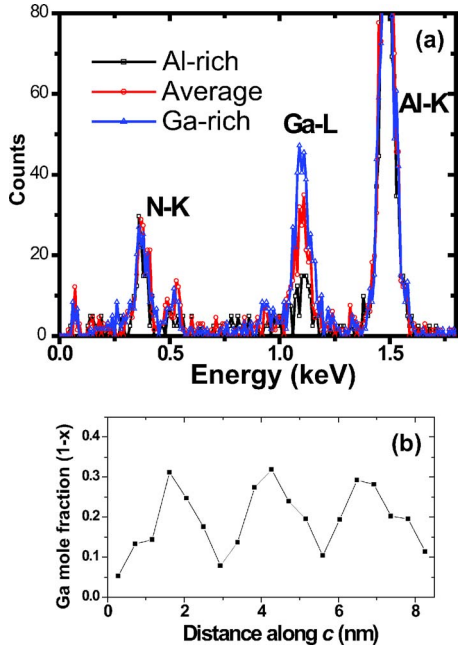

FIG. 4. (Color online) (a) High spatial resolution EDS from Al-rich layers, Ga-rich layers, and large area. (b) Variation of Ga/Al ratio along the c axis.

fraction by triple-axis XRD scan) as standard sample. In general, TEM observations on the AlGaN samples with different AlN mole fractions showed a much stronger tendency to form superlattices at high versus low ($x \leqslant 0.5$) Al concentration. Thus, we observed no modulation for sample 1 ($x=0.25$) but well-defined 13 ML modulation (26 ML for one unit cell) for sample 10 ($x=0.97$) (Fig. 5). For sample 10, the measured Al maximum and minimum were 0.993 and 0.892, respectively.

Figure 6(a) displays a typical symmetric XRD $\omega/2\theta$ scan from a strongly modulated AlGaN film ($x=0.65$), in which the (0002) diffractions of AlGaN and AlN buffer layer can be clearly separated. The small angle peak (O1) corresponds directly to the modulation period. Note that, if 1:1 ordering was present, it would produce a peak at ~9°, but no such peak is present. The two first order satellite peaks (O2 and O3) around the (0002)AlGaN fundamental reflection are very different in their intensities, implying strong interference between compositional and strain modulations.[36] Figure 6(b) shows small angle modulation-related peaks from samples with $x=0.5$, 0.65, and 0.8. Consistent with the TEM results, our XRD results show well-defined modulation with single modulation period for each wafer (central area). For example, we measured the full width at half maximum (FWHM) of the O1 peak from sample 6 ($x=0.65$) to be 0.085° in high resolution double-axis scan, the same as that of AlGaN (0002).

Although the modulation amplitude of such superlattices is difficult to quantify by XRD, we can evaluate the relative modulation amplitude by comparing the intensities of the O1 peaks [Fig. 7(a)] or the intensity ratios between the O2 peaks and (0002)AlGaN peaks [Fig. 7(b)]. XRD results showed the same variation of modulation amplitude as TEM observations. For $x=0.25$, very weak peaks corresponding to 12 ML modulation could only be observed for very strong incident x-ray intensity. With the increase of AlN mole fraction, the intensities first increased slowly from $x=0.25$ to 0.50, then increased abruptly from $x=0.50$ to 0.65, and then remained high from 0.65 to 0.80. Modulation period decreased from 12 to 10 ML from $x=0.25$ to 0.80. Both XRD and electron diffraction showed much weaker modulation-related peaks for $Al_{0.97}Ga_{0.03}N$ compared to other high Al concentration samples, which is attributed to the weak modulation of both strain and composition at very low Ga concentration. The variation of the XRD peak intensity for samples around $x=0.5$ and 0.8 [Figs. 7(a) and 7(b)] indicates that the modulation amplitude is very sensitive to the growth condition and may vary to a large degree even for samples with very similar composition. For example, the intensity of the modulation-related peak of sample 4 ($x=0.48$) is only about half of those for samples 3 and 5, while sample 8 ($x=0.8$) gives much stronger satellite peaks compared to the other two samples with $x \sim 0.80$. Figures 7(a) and 7(b) are very consistent over the full alloy series and show that the modu-

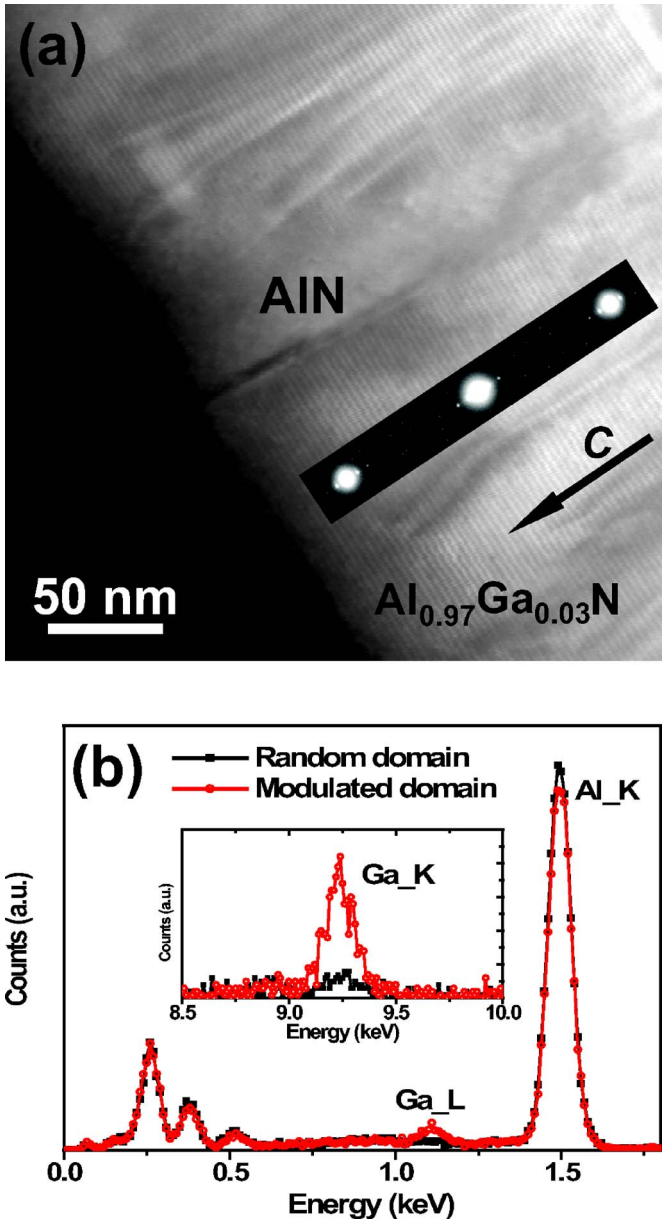

FIG. 5. (Color online) (a) Low magnification cross-sectional Z-contrast image of sample 10 (x=0.97). The inset is a diffraction pattern of the AlGaN film. (b) EDS spectra from the random domain and a modulated domain indicating that the random domain is pure AlN.

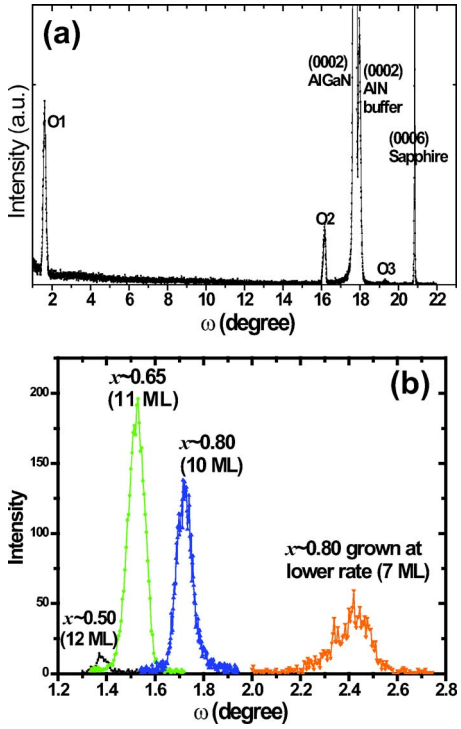

FIG. 6. (Color online) (a) A typical XRD $\omega/2\theta$ scan. (b) Comparison of the superlattice-related small angle XRD satellite peaks from samples with x =0.5 (12 ML modulation period), 0.65 (11 ML), and 0.80 (10 ML) grown at ~400 nm/h. The satellite peak from an $x\sim0.80$ AlGaN sample grown at a rate of ~290 nm/h indicates a reduced modulation period at 7 ML.

lation amplitude in high Al concentration AlGaN (samples 6–9) is much stronger than that in low Al concentration AlGaN (samples 1–5). The only exception is that though both Figs. 7(a) and 7(b) show that samples 6 and 8 have the strongest satellite peaks, sample 6 has the strongest O1 peak while sample 8 has the highest relative O2 peak. This discrepancy may be caused by the high surface sensitivity of the small angle O1 peak which can be largely affected by small XRD misalignment due to poor surface qualities and slight film bending. Surface-sensitive low-energy secondary electron imaging (not shown) demonstrated that sample 6 had considerable less surface structural features than sample 8, indicating a better surface quality for sample 6 (x=0.65).

The spontaneous superlattice structure also displayed a dependence on the wafer's radial location. For each sample, the central 1 in. diameter area of the wafer, where the above results were taken, was homogeneous in both modulation amplitude and modulation period. The modulation period decreased gradually with increasing distance from the wafer center, while the modulation amplitude increased dramatically in the low ($x\leqslant0.5$) Al mole fraction samples but remained relatively constant across the whole wafer in high ($\geqslant0.65$) Al mole fraction samples. Figure 8 shows XRD scans from wafer center and wafer edge areas in sample 5 (x=0.5). The modulation period dependence on radius proves that the spontaneous superlattice did not originate from rotation of the wafer. As a counterexample, rotation

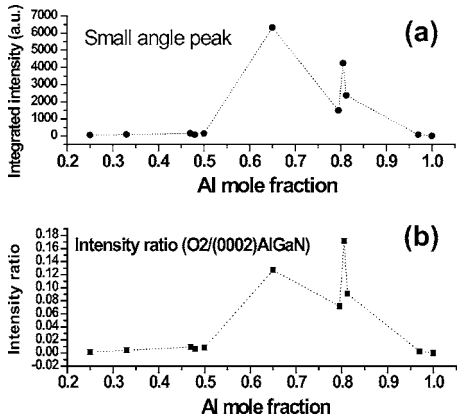

FIG. 7. (a) Integrated intensity of the small angle satellite peaks vs Al mole fraction. (b) Intensity ratio between O2 and AlGaN(0002) vs Al mole fraction.

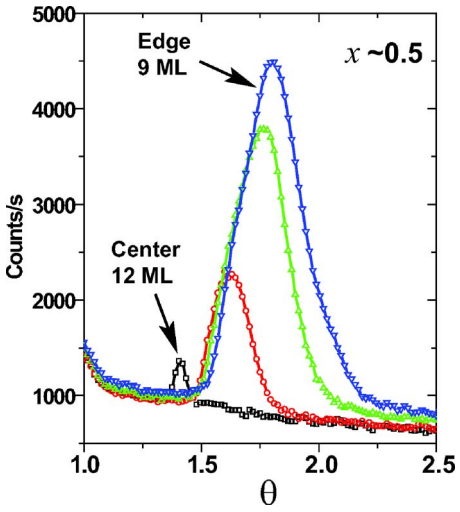

FIG. 8. (Color online) XRD scans ($\theta/2\theta$) of the small angle satellite peaks in different locations of a single AlGaN wafer with $x=0.5$. The modulation period decreased gradually with increasing distance from the wafer center, while the modulation amplitude increased abruptly.

effects introduced sinusoidally modulated $ZnSe_xTe_{1-x}$ superlattices in the presence of an inhomogeneous distribution of constituent fluxes, with a *constant* modulation period controlled by the rotation speed.[37] For the $Al_xGa_{1-x}N$ reported here, the increase in modulation amplitude with radius is likely due to a slight temperature decrease (20–30 °C) at the wafer edge.

Our preliminary results on the effect of growth rate show that the modulation period decreases with decreasing growth rate. For group-III-rich condition, the growth rate depends on the nitrogen flux.[4] In our initial attempt, an AlGaN film was grown at a lower nitrogen flux. The AlN mole fraction was determined to be ~0.80 by XRD. The growth rate was estimated to be ~290 nm/h compared to ~400 nm/h for samples 1–11 by using N flux=(Al flux)/x (Ref. 4) and directly measuring the film thicknesses using cross-sectional SEM. Using XRD, the modulation period was determined to be 7 ML in contrast to 10 ML period observed for samples with similar composition grown at a rate of ~400 nm/h. On the other hand, similar satellite peak intensities were observed by XRD in this low growth rate sample compared to samples 7 and 9.

B. Phase separation

Besides the atomic compositional superlattice, the AlGaN films exhibited phase separation. Figure 9(a) and 9(b) show high resolution double- and triple-axis XRD $\omega/2\theta$ scans of AlGaN samples with different AlN mole fractions. For samples with $x=0.25$ and 0.50, the splitting of the (0002)AlGaN peaks is a direct indication of phase separation. Similarly, splitting was also observed in the NBE CL spectra of these two samples [Fig. 10]. For $x=0.25$, the AlN mole fractions of the two phases calculated from the splitting of the XRD (0002) diffraction peaks were 0.198 and 0.266, which match those (0.186 and 0.261) derived from the NBE emission peaks closely.

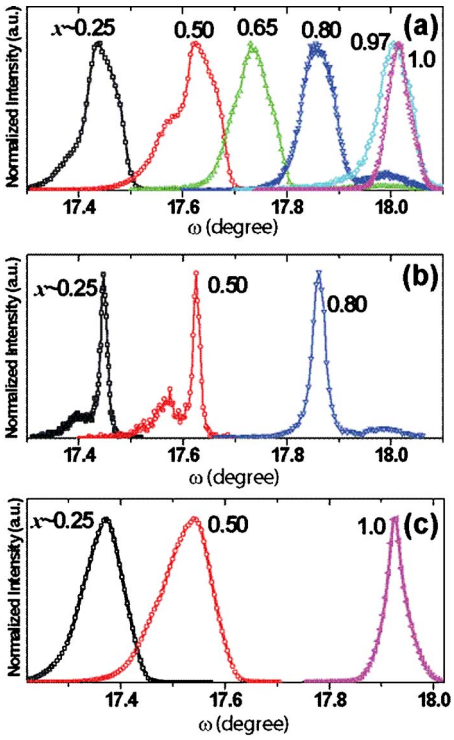

FIG. 9. (Color online) (a) Double-axis XRD scans of AlGaN(0002) of several mole fractions. (b) Triple-axis XRD scan of AlGaN(0002) of $x=0.25$, 0.50, and 0.80. (c) Double-axis XRD scans using a slightly lower resolution diffractometer setup.

We obtained spatial maps of the domain sizes using CL to measure individual peak intensity versus wafer location. Figures 11(a) and 11(b) show CL intensity maps corresponding to the two NBE peaks in the $x=0.25$ sample, which confirm that they were from spatially separated regions. Direct measurement from the CL maps showed that domain sizes of the secondary phase were up to ~300 nm. For $x=0.5$, no

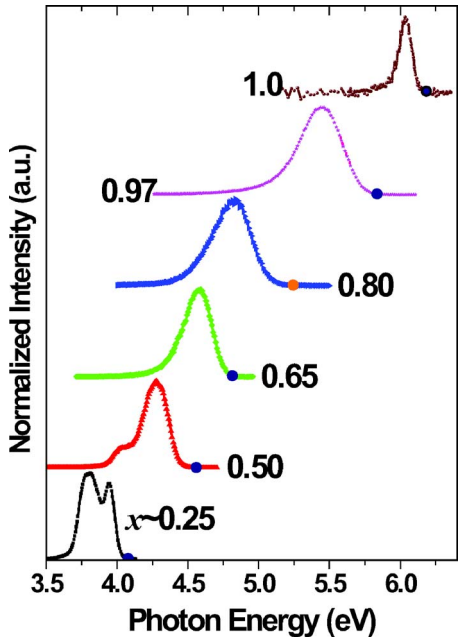

FIG. 10. (Color online) CL NBE emissions vs Al mole fraction. The onset energy is marked for each emission spectrum.

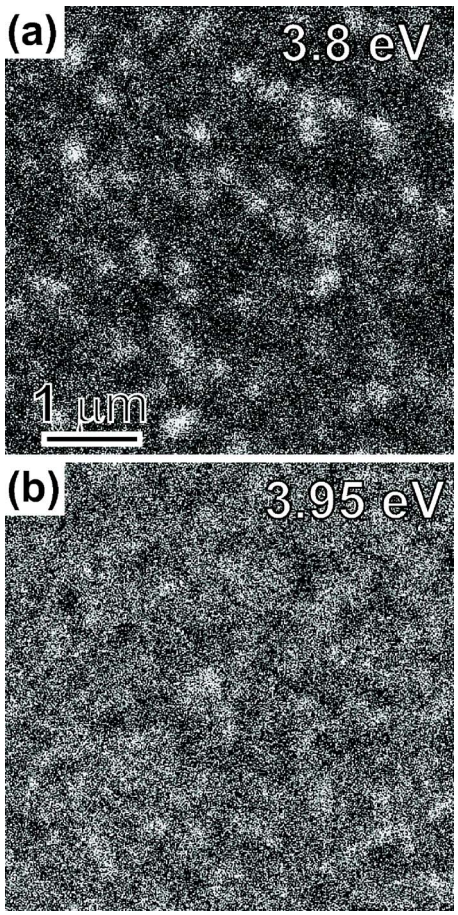

FIG. 11. (Color online) CL images of sample 1 with $x=0.25$ using the two split NBE peaks at 3.80 eV (a) and 3.95 eV (b), respectively.

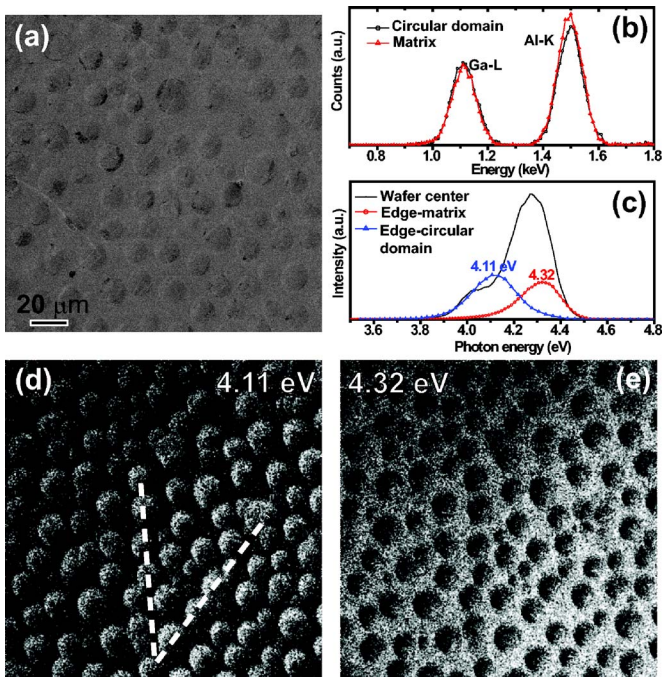

FIG. 12. (Color online) (a) SE image of area close to the edge of wafer with $x=0.5$ showing array of circular domains. (b) EDS spectra from domain areas and matrix showing lower Al content within circular domains. (c) CL spectra on and between circular domains showing lower NBE emission energy on vs matrix (between circular domains). (d) CL maps at $h\nu=4.11$ eV showing lower emission energy of circular domains. Superimposed lines indicate hexagonal arrangement of domains. (e) CL map at $h\nu=4.32$ eV showing higher emission energy between circular domains.

distinguishable domains were observed, indicating a dramatic domain size decrease with AlN mole fraction increase. For $x \geqslant 0.65$, phase separation was almost totally suppressed. Instead, strong spontaneous composition modulation appeared. Conversely, no significant composition modulation was evident for $x \leqslant 0.50$. The composition difference of the separated phases in AlGaN is much smaller than in InGaN. Thus, the separated XRD peaks can be easily overlooked by using even a slightly lower resolution XRD setup. For example, the asymmetric shapes of the (0002)AlGaN cannot be easily identified for both samples with $x=0.25$ and 0.50 in the high resolution double-axis XRD scans using the two bounce Philips X'pert diffractometer [Fig. 9(c)]. Using pure (0002)AlN as a reference, the peak counts of the Philips X'pert was about 20 times that of the Bede, and the full widths at half maximum (FWHM) and 5% maximum of the XRD peak from the two diffractometers were 0.048° and 0.11° for the Bede versus 0.042° and 0.13° for the Philips X'pert.

TEM results showed that the separated phases were very similar in terms of spontaneous modulation. In contrast to the reported coexistence of domains with and without 1:1 ordering structure in InGaN,[12] we did not observe coexistence of modulated and random AlGaN domains. One apparent exception was that $Al_{0.97}Ga_{0.03}N$ exhibited very small domains (<1% in volume, <50 nm in width) without modulation, but these domains were determined to be pure AlN using EDS (Fig. 6), which indicated that small local composition variation existed even at very high AlN mole fraction.

The domain size of the secondary phase was found to increase dramatically in the region close to wafer edges. Surface-sensitive secondary electron (SE) images from regions close to wafer edges showed clear micron-sized circular domains. Figure 12 illustrates these domains and their difference in composition. Figure 12(a) is a SE image from the outer region of the AlGaN wafer with $x=0.5$. Figure 12(b) shows EDS spectra from the domains and the matrix between these domains, respectively, which were taken in another SEM equipped with an EDS spectrometer. The Al mole fractions of the secondary domains and the matrix were determined to be 50% and 54% using sample 1 ($x=0.245$) as standard. Figure 12(c) compares micro-CL spectra from the circular domains and surrounding matrix with the CL spectrum from wafer center. These spectra indicate different emissions energies for the domains versus their surrounding. The circular domains exhibit characteristic emission at ~4.11 eV while the surrounding matrix shows emission predominantly at 4.32 eV. CL intensity maps at 4.11 and 4.32 eV are shown in Figs. 12(d) and 12(e), respectively. The emission energy difference between the domains and the matrix was observed to be around 200 meV, corresponding to ~7% difference in Al mole fraction which is consistent with triple-axis XRD result (not shown) that determines the Al mole fractions of the two separated phases to be 0.48 and 0.545, respectively. The smaller difference (4%) observed using EDS is believed to be due to the effect of backscattered

electrons which may excite x ray from a large volume and reduce the composition contrast. The increase in Al mole fraction from 0.50 at the wafer center to ~0.545 at the wafer edge may be attributed to the slight decrease of N partial pressure or the cooler temperature at the wafer edge. Though the composition difference between such large domains and the matrix matches the phase separation in the wafer center [Fig. 12(c)], the formation mechanism of these huge circular Ga-rich domains might be different from the phase separation considering the huge size and distribution location of these separated domains. Since they were observed only in the region near the wafer edge where the temperature was lower than the wafer center, it is possible that they simply originate from Ga droplet formed at the wafer edge during growth.

Taken together, these results indicate unambiguously that AlGaN separates into phases with different compositions, ruling out the possibility that the splitting of the XRD and CL spectra is caused by strain between the AlGaN films and the AlN buffer layers. Additional evidence contradictory to strain-induced peak splitting includes the following: (i) CL spectra obtained with 1 keV incident beams probe only the first few nanometers[38] yet also display the same peak splitting. If the peak splitting was due to inhomogeneous strain within the film, our depth-resolved CL would have shown differences between the bulk and the surface. (ii) If the (0002)AlGaN XRD peak splitting was due to strain, then it should decrease monotonically with increasing Al concentration and decreasing strain, yet Fig. 9(b) shows that the secondary peak (corresponding to lower Al concentration) for $x=0.50$ is ~40% of the total (0002) peak intensity, higher than the ~30% for $x=0.25$.

C. Near band edge CLS at high Al concentration

Figure 10 shows the low-temperature NBE emission of the as-grown plan-view AlGaN samples with $x=0.25$, 0.5, 0.65, 0.80, 0.97, and 1. In order to establish the uniformity of the CL emissions on a microscopic scale, we performed low-temperature CLS using thin TEM cross-sectional specimens for samples 8 ($x=0.8$) and 10 ($x=0.97$). Unlike bulk samples, ultrathin (<100 nm) TEM samples limit the spread of the electron cascade and backscattered electrons to the sample thickness. Coupled with the nanometer-scale minority carrier diffusion lengths in GaN alloys,[39] a practical spatial resolution below 30 nm can be obtained for incident beam energies of 5–10 keV. For example, in the TEM specimen with $x=0.97$, the AlN domain and the adjacent AlGaN domains (shown in Fig. 5) could be identified using such nano-CLS. The NBE emission spectra from nanometer-sized areas in both TEM specimens showed rather uniform emissions consistent with the emissions observed in the as-grown plan-view samples. Figure 13 shows the comparison between representative CL spectra from the TEM thin specimen and the as-grown plan-view films. At low temperature, the NBE emission of AlGaN is dominated by the Si-donor bound exciton transition, while the high-energy onset of the NBE emission (E_0) tracks the band gap.[34,41] For AlN ($x=1$), the measured emission peak energy and band gap are 6.035 and 6.178 eV, respectively, which are consistent with previous reports.[41,42] The CL-measured band gap of epitaxial AlN film is usually smaller than that measured by absorption—6.28 eV.[43] Figure 10 shows that when x decreases from 1 to 0.97, the CL peak energy decreases by ~600 meV. Figure 14 shows the deviation of the CL NBE peak energies E_X from the calculated I_2. To calculate the theoretical emission peak energies, the following parameters were used: $E_g^{(\mathrm{AlN})}=6.178$ eV, $I_2^{(\mathrm{AlN})}=6.035$ eV (donor bound exciton energy $DX^0=135$ meV) and $E_g^{(\mathrm{GaN})}=3.504$ eV, $I_2^{(\mathrm{GaN})}=3.476$ eV ($DX^0=28$ meV).[40] We assume a linear dependence of the donor binding energy relative to the band gap on the Al mole fraction. The experimental emission energies fit the theoretical I_2 closely at low Al concentration and in pure AlN but are considerably lower for Al-rich samples. The emission energy reduction exceeds 300 meV for $x \geqslant 0.65$ with a maximum of 525 meV for sample 8 ($x=0.80$). Besides the emission peak energies, the NBE emission onsets E_0 also display large deviations from calculated values in Al-rich AlGaN samples. Figure 15(a) shows the measured E_0 as a function of Al mole fraction. E_0 is obtained from an extrapolation of the high-energy emission to the base line. The calculated band gap for $E_g^{(\mathrm{AlN})}=6.178$ eV and $E_g^{(\mathrm{GaN})}=3.504$ eV with bowing parameters of both $b=0$ and 1 are also shown for comparison. Figures 15(b) shows the difference between the calculated band gap, E_g ($b=1$) and E_0. Generally, for samples with $x \leqslant 0.5$, the measured band gaps are close to or

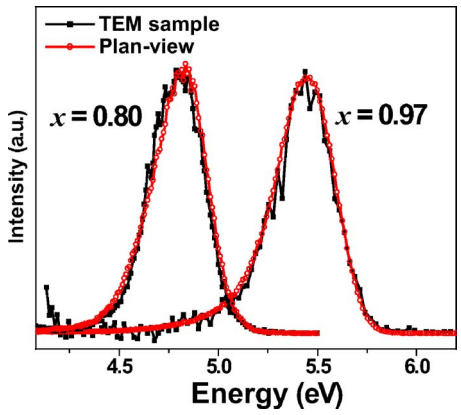

FIG. 13. (Color online) Comparison of nano-CL spectra from $Al_{0.97}Ga_{0.03}N$ and $Al_{0.8}Ga_{0.2}N$ cross-sectional TEM specimens with CL spectra from as-grown plan-view samples.

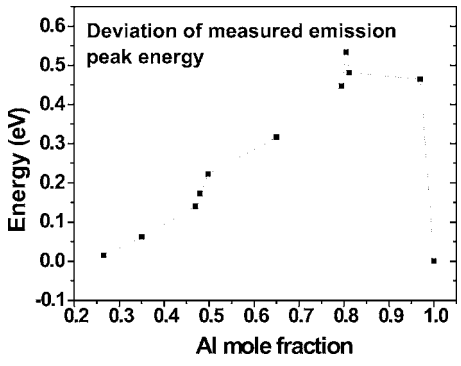

FIG. 14. Deviation of measured emission peak energies E_x from calculated I_2 with $b=1$ vs Al mole fraction.

slightly higher (up to ~100 meV) than the E_g (b=1) values, while for specimens with $x \geqslant 0.65$, the E_0 are considerably lower (up to 257 meV) than E_g (b=1). For b=0, the trend remains the same, i.e., the deviation of the measured band gap from theoretical value becomes larger with increasing Al mole fraction. In addition, it is noticed that the measured band gaps may vary dramatically in those samples with similar Al mole fraction, e.g., samples 3–5 around $x \sim 0.5$ and samples 7–9 around $x \sim 0.8$ in Table I. The emission uniformity of both TEM samples in ~30 nm scale ruled out the existence of preferential recombination regions with much lower emission energy than other areas and confirmed that the Al-rich samples have lower band gaps and emission peak energies compared to the expected values for random AlGaN.

IV. DISCUSSION

A. Correlation of near band edge emissions with composition modulation

The uniform modulation of composition shown by TEM and XRD, coupled with the reductions of band gap and NBE emission energies shown by CLS, suggests the formation of spontaneous superlattices in AlGaN. The band gap reduction versus Al mole fraction shown in Fig. 15(b) is very consistent with the modulation amplitude indicated by XRD (Fig. 7) and TEM (Fig. 5). In those samples with very similar compositions, i.e., x=0.5 in samples 3–5 and x=0.8 in samples 7–9, the band gap reductions match the modulation amplitudes very closely. In addition, since the modulation amplitude increases dramatically from the wafer center to the wafer edge in low Al concentration samples (Fig. 8), the effect of modulation amplitude for the same wafer can be studied for samples with similar Al concentration and almost the same impurity levels of Si and O. CL and XRD results from pieces in different wafer positions in sample 1 (x=0.25) and sample 5 (x=0.50) confirmed that high modulation amplitude causes larger band gap reduction. Conversely, ~5% increase in Al mole fraction was observed for the edge area of sample 5 (x=0.5), so ~140 meV increase is expected for the band gap and emission energy; however, the observed increases for both are <50 meV [Fig. 12(c)].

To first order, the band gap reduction can be understood as electron-hole pairs preferentially recombining in local regions with lower band gap, i.e., relatively Ga-rich layers. Indeed, for x=0.80 and 0.97, CLS NBE energies correspond to Al compositions of x=0.637 and 0.841, respectively, closely matching the high spatial resolution EDS results (0.679 and 0.892, respectively).[31] However, more precise calculations should take into account not only composition but also quantum confinement, strain, and tunneling. To fully understand the influence of such spontaneous compositional superlattice on the optical properties, first-principles calculations have been carried out to model the electron and hole miniband energies.[44] Preliminary calculation results integrated in Figs. 15(a) and 15(b) show calculated band gaps and band gap shifts for the maximum possible Al compositional fluctuation in the superlattice (set by the condition $0 < x_{Al} < 1$) along with the case of "40% modulation" for

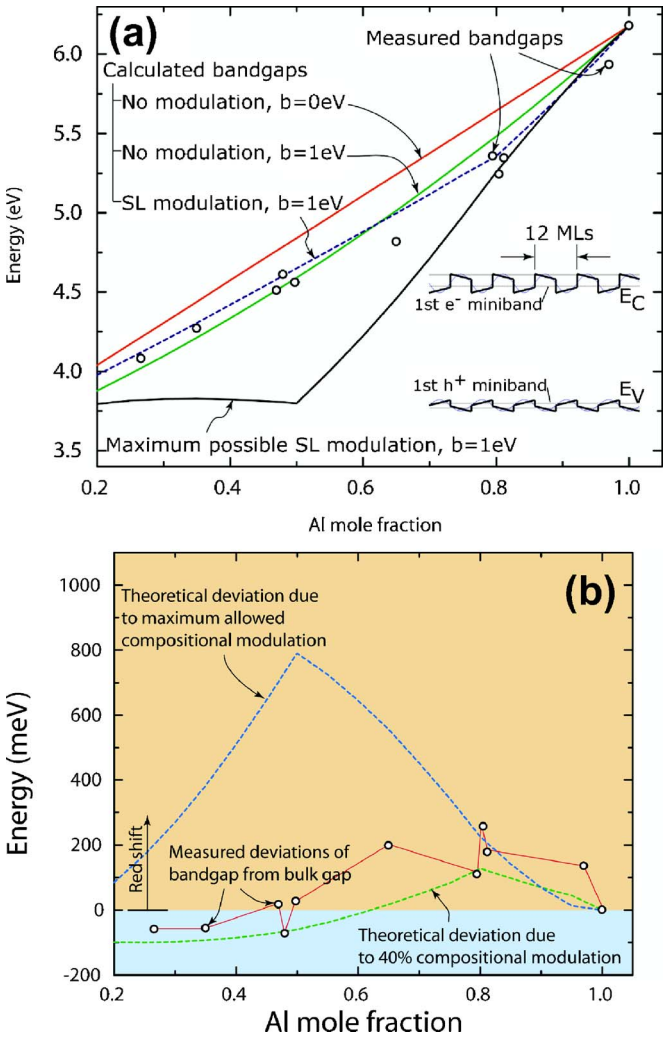

FIG. 15. (Color online) (a) Comparison of CL-measured emission onsets E_0 with calculated band gaps E_g for bowing parameter b=0 and 1 vs Al mole fraction, and the theoretically calculated band gaps using the superlattice miniband model. (b) Experimental deviation of E_0 from E_g with b=1 vs Al mole fraction shown along with calculated deviations using the superlattice miniband model.

which the compositional fluctuation was set to 40% of the AlN mole fraction (x) for $x \leqslant 0.8$ and decreases linearly from 40% to 0% for $0.8 < x \leqslant 1$. The effect of spontaneous and piezoelectric polarization on the energy bands was incorporated.[45] The miniband calculations were performed in an effective mass approximation of the Schrödinger equation, and the effective band gaps were thereafter evaluated from the difference of the electron and hole miniband energies.[46] The inset in Fig. 15(a) is a typical calculated band diagram of the superlattice with the miniband energies. Note that a "square-wave" modulation in composition is used as a close approximation to the experimental modulation in Fig. 3(c). The calculated shifts in band gap for the 40% modulation fit both the trend and the magnitudes of the experimental data to a reasonable accuracy in Figs. 15(a) and 15(b). Especially, the calculated band gap of the superlattice is blueshifted for average Al compositions lower than x=0.62 and redshifted for compositions above it. Interestingly, this behavior is also observed experimentally. This indicates that the effect of spontaneous superlattice formation on the elec-

tronic and optical properties of the alloys can be explained by the electron and hole miniband model of the superlattice electronic states. On the other hand, it is clearly highlighted in Figs. 15(a) and 15(b) that for large compositional fluctuations, the band gap is redshifted with respect to the bulk gap. Experiments and calculations also revealed similar reductions in band gaps and emission peak energies for spontaneous superlattice in $ZnSe_xTe_{1-x}$ epilayers[47,48] and 1:1 ordering in III-V ternary alloys[7,49] and AlGaN.[28,30,32]

As with the emission onsets in Fig. 15(b), the deviation of the NBE emission peak positions (Fig. 14) increases with increasing Al mole fraction. The redshift reaches >300 meV around $x=0.65$ with a maximum of 533 meV for $x=0.80$. Such redshift is much higher than the band gap reduction. Thus the difference between E_X and E_0 can be >450 meV. This may also be interpreted in terms of minigap formation in the spontaneous superlattice.

Impurities may also affect the observed band gap reduction in our Si-doped AlGaN. Nam *et al.* has interpreted their gradually increased redshifts of the I_2 emission line and free excitons with increasing Si doping concentration in terms of a Si-induced band gap renormalization (reduction).[42] However their band gap decreased by only ~30 meV with Si doping increasing from $1.5\times10^{17}/cm^3$ to $1.5\times10^{18}/cm^3$—almost ten times lower than the results presented here. In addition, we observed large band gap reduction only in Al-rich AlGaN samples but not in pure AlN with very similar or even higher Si doping level. This result rules out the possibility that our large band gap reductions are due to high level Si doping. Moreover, comparison of the band gap reductions shown in Fig. 15(b) and the Si doping concentrations in Table I also shows no correlation. Similarly, no close correlation has been found between band gap reduction and O concentration or Si+O. Oxygen is a critical impurity for Al-rich AlGaN since Al has a large affinity for oxygen. Though a very low-O MBE chamber has been used in the growth,[33] high oxygen impurity level has been observed using SIMS in Al-rich AlGaN samples. O-related deep-level states has been identified by depth-resolved CLS in Al-rich AlGaN samples in our previous study,[34] but we did not find evidence for O having a strong influence on the NBE emission. For example, in sample 10 ($x=0.97$), the surface region has considerably higher O than the bulk and exhibited a 4.76 eV deep-level emission,[34] but the NBE emissions from surface region and bulk were almost the same.

B. Driving force for alloy-dependent compositional inhomogeneity

Phase separation is considered unlikely in AlGaN due to the small lattice mismatch between AlN and GaN. Calculations based on different approaches have shown that AlGaN is miscible in typical growth temperatures and the critical temperature for spinodal decomposition is very low.[14,16–18] In contrast, the InGaN alloy has been shown by both calculation[15–18] and experiment[9] to be thermodynamic unstable for typical growth temperatures, and phase separation is spinodal in nature. However, most currently available calculations were based on cubic (zinc blende) structure AlGaN. The lattice mismatch between cubic AlN and GaN is ~3.2%, which is higher than that for a nonpolar axis of wurtzite AlGaN but significantly smaller than the 4.1% *c*-axis mismatch of wurtzite AlGaN.

Our results showed unambiguous evidence of phase separation in AlGaN films, which introduces splitting of the UV emission peak and can affect optical applications. Collins *et al.*[50] and Sampath *et al.*[50] have proposed that nanoscale compositional inhomogeneities can enhance luminescence efficiency, which is consistent with our observation in $x=0.25$ AlGaN (Figs. 10 and 11) showing that the emission intensity from the secondary low Al phase is considerably stronger than that from the majority high Al phase. We also showed that the compositional variation due to phase separation in AlGaN is much smaller compared to that in InGaN and could be easily overlooked by a low resolution double-axis XRD scan. This suggests that the driving force for phase separation in AlGaN has been underestimated. Recently, Sun *et al.* reported that phase separation was enhanced for higher temperature growth of AlN interlayers between MOCVD-grown AlGaN on micron-thick GaN substrates,[51] a result attributed to an inhomogeneous distribution of strain and Al composition in the high-temperature interlayer. Figure 12(d) illustrates the rough alignment of the secondary domains along particular directions, which may imply that strain is involved in the phase separation. However, we found slightly larger phase separation for samples with $x=0.5$ vs $x=0.25$, which is inconsistent with such strain-induced phase separation. Further work is needed to clarify the kinetic and thermodynamic characteristics of the phase separation in AlGaN epilayers.

Our results show clearly that the spontaneous modulation is atomic compositional modulation. It has been shown in cubic III-V alloys that spontaneous long range ordering/compositional modulation is not driven by bulk thermodynamics but by surface or near surface phenomena.[6–8] So surface kinetic factors are expected to play important roles in such atomic compositional modulation. Previous work already showed that the periods of the spontaneous ordering/modulation in AlGaN strongly depend on growth conditions. Iliopoulos *et al.* reported that the 1:1 ordering in MBE-grown AlGaN films was preferred under N-rich growth conditions, while group-III-rich conditions favored longer period modulation.[24] Strittmatter *et al.* varied the modulation period from 5.5 to 8.3 nm by increasing the growth rate from 1.4 to 2.5 μm/h using MOCVD.[29] Recently, Albrecht *et al.* adapted a growth model for 1:1 ordering originally proposed for InGaN into AlGaN, which suggested that the system can minimize its energy by incorporating Al and Ga selectively to the two group III sites on $\{1\bar{1}01\}$ facets.[30] There is no available detailed model for the compositional modulation thus far, but some reports seem to support a general model for self-organized semiconductor alloy superlattices, suggesting that differences in atomic sizes and diffusion mobilities of the alloyed atoms could generate modulated tensile strain and compressive strain at the growth surface and introduce spontaneous superlattice close to growth direction.[52] This model predicted a small deviation between the growth direction and the superlattice direction, which was observed in

AlGaN superlattices by Iliopoulos *et al.*[24] However, this model suggested that increasing the growth rate induces shorter superlattice period, which is contradictory to the experimental results by Strittmatter *et al.*[29] and in our study.

In this study, we demonstrate that the spontaneous modulation in AlGaN varies systematically with the AlN mole fraction; meanwhile the growth rate and temperature have strong influences. In contrast to the dramatic change of modulation amplitude, the modulation period observed in the wafer central areas only varies from 12 ML (~3 nm) to 10 ML (~2.5 nm) with increasing AlN mole fraction from 0.25 to 0.8 when the growth rate is constant, which suggests that the modulation period is not sensitive to the composition. However, our results may indicate that the modulation period is very sensitive to the growth rate and decreases from 10 ML (~2.5 nm) to 7 ML (~1.75 nm) almost proportionally for $x \sim 0.80$ with growth rate decreased from ~400 to ~290 nm/h, which is similar to the observation by Strittmatter *et al.*,[29] even though the latter case employed MOCVD and very different growth conditions.

Our observation has indicated that the spontaneous modulation has a radial dependence, i.e., the modulation period decreases largely in the near wafer edge area, and for $x \leqslant 0.5$, the modulation amplitude increases dramatically near the wafer edge. Under group-III-rich growth condition, the growth rate is determined by the N flux and the AlN mole fraction is determined by Al flux/N flux.[4] The plasma N source may introduce a slight decrease of N flux near the wafer edge, which may lead to a decrease of growth rate and therefore a shorter modulation period near the edge. However, the increase in AlN mole fraction from the wafer center to the wafer edge has been found to be only ~5%, leading to an ~5.3% decrease in N flux and thus the growth rate. Such slight change is believed not sufficient to cause the dramatic changes in both modulation period and amplitude. We tend to believe that the main reason for the radial dependence, especially the pronounced enhancement of modulation amplitude for low Al concentration AlGaN near the wafer edge, is the 20–30 °C decrease in temperature from the wafer center to the wafer edge. The growth temperature has been shown to have a major influence on the degree of spontaneous long range ordering in III-V alloys.[6–8] The influences of growth temperature and growth rate on the spontaneous superlattice structure in AlGaN still need to be studied systematically.

The complementary dependence of compositional modulation and phase separation on AlN mole fraction observed in this study suggests that the different diffusion behaviors of Ga and Al play an important role. Al has much stronger bonding with N and much less mobility compared to Ga. For Al-rich AlGaN, the slower diffusing Al atoms dominate subsequent growth and cooling so that surface compositional modulation is more likely to remain intact. At low Al concentration, the faster Ga diffusion dominates. This facilitates phase separation requiring longer diffusion length.

In addition to the large UV wavelength shift, the spontaneous superlattice has possible application to light emitting diodes where longer wavelength emission can occur from a short period superlattice bounded by bulk AlGaN with the same lattice constant.[31] Lateral confinement due to index of refraction could be reduced, thus raising vertical light emission efficiency.

V. CONCLUSION

In conclusion, the compositional inhomogeneity in MBE-grown AlGaN epilayers and its effects on optical emission have been studied by TEM, XRD, and CLS, which reveal spontaneous modulation, phase separation, and band gap reductions varying systematically with AlN mole fraction across the full alloy series. At low AlN mole fraction ($x \leqslant 0.5$), AlGaN epilayers display pronounced phase separation. With increasing AlN mole fraction, phase separation is strongly suppressed by the formation of spontaneous modulation, in which high spatial resolution TEM techniques unambiguously determine to be atomic-scale compositional superlattices. The pronounced reductions in band gaps and emission energies exceeding several hundred meV for the Al-rich AlGaN can be understood in terms of spontaneous superlattice formation.

ACKNOWLEDGMENTS

One of the authors (L.J.B.) gratefully acknowledges support from the Office of Naval Research (Colin Wood) and the Department of Energy (Jane Zhu), two of the authors (L.J.B. and S.A.R.) from the National Science Foundation (Verne Hess), and another author (W.J.S.) from the National Science Foundation (Fil Bartoli). The experiments using JEOL 2010F TEM and Philips X'pert XRD were performed in the Center for Microanalysis of Materials, University of Illinois, which is partially supported by the U.S. Department of Energy under Grant No. DEF02-91-ER45439.

[1] R. D. Dupuis and J. C. Campbell, in *Wide Energy Bandgap Electronic Devices*, edited by F. Ren and J. C. Zolper (World Scientific, Singapore, 2003), p. 429.
[2] T. D. Moustakas, E. Iliopoulos, A. V. Sampath, H. M. Ng, D. Doppalapudi, M. Misra, D. Korakakis, and R. Singh, J. Cryst. Growth **227–228**, 13 (2001).
[3] M. A. Khan, M. Shatalov, H. P. Maruska, H. M. Wang, and E. Kuokstis, Jpn. J. Appl. Phys., Part 1 **44**, 7191 (2005).
[4] R. Averbeck and H. Riechert, Phys. Status Solidi A **176**, 301 (1999); E. Iliopoulos and T. D. Moustakas, Appl. Phys. Lett. **81**, 295 (2002).
[5] S. R. Lee, A. F. Wright, M. H. Crawford, G. A. Petersen, J. Han, and R. M. Biefeld, Appl. Phys. Lett. **74**, 3344 (1999).
[6] A. Zunger, in *Handbook on Semiconductors*, edited by T. S. Moss (Elsevier Science, New York, 1994), p. 1399.
[7] A. Zunger, MRS Bull. **22**, 20 (1997); G. B. Stringfellow, *ibid.* **22**, 27 (1997).
[8] *Spontaneous Ordering in Semiconductor Alloys*, edited by A. Mascarenhas (Kluwer Academic, Dordrecht, Plenum, New York, 2002).
[9] D. Doppaiapudi, S. N. Basu, K. F. Ludwig, Jr., and T. D. Moustakas, J. Appl. Phys. **84**, 1389 (1998).
[10] P. Ruterana, G. Nouet, W. Van der Stricht, I. Moerman, and L. Considine, Appl. Phys. Lett. **72**, 1742 (1998).
[11] M. K. Behbehani, E. L. Piner, S. X. Liu, N. A. EI-Masry, and S. M. Bedair, Appl. Phys. Lett. **75**, 2202 (1999).
[12] D. Doppalapudi, S. N. Basu, and T. D. Moustakas, J. Appl. Phys. **85**, 883 (1999).
[13] J. E. Northrup, L. T. Romano, and J. Neugebauer, Appl. Phys. Lett. **74**, 2319 (1999).
[14] E. A. Albanesi, W. R. L. Lambrecht, and B. Segall, Phys. Rev. B **48**, 17841 (1993).
[15] I. Ho and G. B. Stringfellow, Appl. Phys. Lett. **69**, 2701 (1996).
[16] L. K. Teles, J. Furthmüller, L. M. R. Scolfaro, J. R. Leite, and F. Bechst-

edt, Phys. Rev. B **62**, 2475 (2000).
[17]T. Takayama, M. Yuri, K. Itoh, and J. S. Harris, Jr., J. Appl. Phys. **90**, 2358 (2001).
[18]J. Adhikari and D. A. Kofke, J. Appl. Phys. **95**, 6129 (2004).
[19]D. Korakakis, K. F. Ludwig, Jr., and T. D. Moustakas, Appl. Phys. Lett. **71**, 72 (1997).
[20]M. Misra, D. Korakakis, H. M. Ng, and T. D. Moustakas, Appl. Phys. Lett. **74**, 2203 (1999).
[21]P. Ruterana, G. De Saint Jores, M. Laügt, F. Omnes, and E. Bellet-Amalric, Appl. Phys. Lett. **78**, 344 (2001).
[22]M. Benamara, L. Kirste, M. Albrecht, K. W. Benz, and H. P. Strunk, Appl. Phys. Lett. **82**, 547 (2003).
[23]E. Iliopoulos, K. F. Ludwig, Jr., T. D. Moustakas, and S. N. G. Chu, Appl. Phys. Lett. **78**, 463 (2001).
[24]E. Iliopoulos, K. F. Ludwig, Jr., and T. D. Moustakas, J. Phys. Chem. Solids **64**, 1525 (2003).
[25]B. Neubauer, A. Rosenauer, D. Gerthsen, O. Ambacher, and M. Stutzmann, Appl. Phys. Lett. **73**, 930 (1998).
[26]M. Laügt, E. Bellet-Amalric, P. Ruterana, and F. Omnès, Phys. Status Solidi B **236**, 729 (2003).
[27]I. Levin, L. H. Robins, M. D. Vaudin, J. A. Tuchman, E. Lakin, M. J. Sherman, and J. Ramer, J. Appl. Phys. **89**, 188 (2001).
[28]D. G. Ebling, L. Kirste, K. W. Benz, N. Teofilov, K. Thonke, and R. Sauer, J. Cryst. Growth **227–228**, 453 (2001).
[29]A. Strittmatter, L. Reissmann, D. Bimberg, P. Veit, and A. Krost, Phys. Status Solidi B **234**, 722 (2002).
[30]M. Albrecht *et al.*, Phys. Rev. B **71**, 035314 (2005).
[31]M. Gao, Y. Lin, S. T. Bradley, S. A. Ringel, J. Hwang, W. J. Schaff, and L. J. Brillson, Appl. Phys. Lett. **87**, 191906 (2005).
[32]S. V. Dudiy and A. Zunger, Phys. Rev. B **68**, 041302(R) (2003).
[33]J. Hwang *et al.*, Appl. Phys. Lett. **81**, 5192 (2002).
[34]S. T. Bradley, S. H. Goss, L. J. Brillson, J. Hwang, and W. J. Schaff, J. Vac. Sci. Technol. B **21**, 2558 (2003).
[35]D. E. Jesson and S. J. Pennycook, Proc. R. Soc. London, Ser. A **449**, 273 (1995).
[36]S. P. Ahrenkiel *et al.*, Phys. Rev. Lett. **75**, 1586 (1995).
[37]P. M. Reimer, J. R. Buschert, S. Lee, and J. K. Furdyna, Phys. Rev. B **61**, 8388 (2000).
[38]L. J. Brillson, J. Vac. Sci. Technol. B **19**, 1762 (2001); A. P. Young *et al.*, J. Electron. Mater. **28**, 308 (1999) (1 keV depth probe in GaN).
[39]L. J. Brillson, T. M. Levin, G. H. Jessen, and F. A. Ponce, Appl. Phys. Lett. **75**, 3835 (1999).
[40]P. B. Perry and R. F. Rutz, Appl. Phys. Lett. **33**, 319 (1978).
[41]N. Teofilov, K. Thonke, R. Sauer, L. Kirste, D. G. Ebling, and K. W. Benz, Diamond Relat. Mater. **11**, 892 (2002).
[42]K. B. Nam, M. L. Nakarmi, J. Li, Y. Lin, and H. X. Jiang, Appl. Phys. Lett. **83**, 2787 (2003).
[43]G. D. Chen, M. Smith, J. Y. Lin, H. X. Jiang, S.-H. Wei, M. A. Khan, and C. J. Sun, Appl. Phys. Lett. **68**, 2784 (1996).
[44]Y. Cao, D. Jena, M. Gao, and L. J. Brillson (unpublished).
[45]F. Bernardini, V. Fiorentini, and D. Vanderbilt, Phys. Rev. B **56**, R10024 (1997).
[46]B. K. Ridley, W. J. Schaff, and L. F. Eastman, J. Appl. Phys. **94**, 3972 (2003).
[47]S. Lee, U. Bindley, J. K. Furdyna, P. M. Reimer, and J. R. Buschert, J. Vac. Sci. Technol. B **18**, 1518 (2000).
[48]G. Yang, S. Lee, and J. K. Furdyna, Phys. Rev. B **61**, 10978 (2000).
[49]L. C. Su, I. H. Ho, and G. B. Stringfellow, Appl. Phys. Lett. **65**, 749 (1994).
[50]A. V. Sampath, G. A. Garrett, C. J. Collins, W. L. Sarney, E. D. Readinger, P. G. Newman, H. Shen, and M. Wraback, J. Electron. Mater. **35**, 641 (2006); C. J. Collins *et al.*, Appl. Phys. Lett. **86**, 031916 (2005).
[51]Q. Sun, *et al.*, Appl. Phys. Lett. **87**, 121914 (2005).
[52]P. Venezuela, J. Tersoff, J. A. Floro, E. Chason, D. M. Follstaedt, F. Liu, and M. G. Lagally, Nature (London) **397**, 678 (1999).